Electronic Supplementary Material (ESI) for Analyst

Multi-functional fluorescent probe for Hg^{2+}, Cu^{2+} and ClO^- based on a pyrimidin-4-yl phenothiazine derivative

Jiena Weng,[a] Qunbo Mei,*[a] Bin Zhang,[a] Yuanzhi Jiang,[a] Bihai Tong,[c] Quli Fan,[a] Qidan Ling[a] and Wei Huang*[a,b]

[a] *Key Laboratory for Organic Electronics & Information Displays and Institute of Advanced Materials, Nanjing University of Posts & Telecommunications, Nanjing 210046, China. Fax: +86 25 8586 6533; Tel: +86 25 8586 6396; E-mail: iamqbmei@njupt.edu.cn (Q. Mei), iamwhuang@njupt.edu.cn, iamdirector@fudan.edu.cn (W. Huang).*

[b] *Jiangsu-Singapore Joint Research Center for Organic/Bio- Electronics & Information Displays and Institute of Advanced Materials, Nanjing University of Technology, Nanjing 211816, China. Fax: +86 25 5813 9988; Tel: +86 25 5813 9001*

[c] *Institute of Molecular Engineering and Applied Chemistry, College of Metallurgy and Resources, Anhui University of Technology, Ma'anshan, Anhui 243002, P. R. China*

Contents:

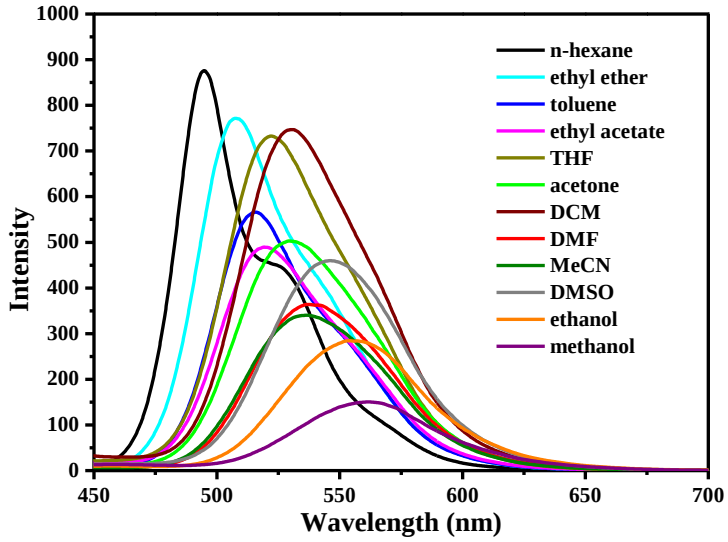

Fig. S1 Photoluminescence spectra (λ_{ex} = 360nm) of **PzDPM** recorded in different solvents.

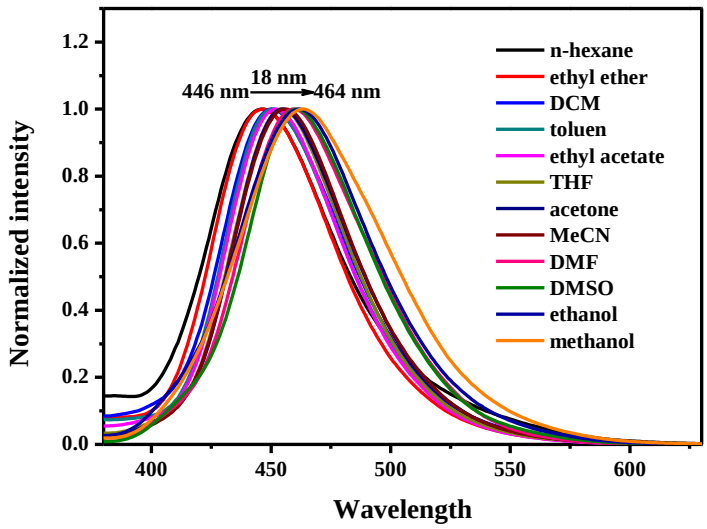

Fig. S2 Normalized photoluminescence spectra (λ_{ex} = 360nm) of **PzODPM** recorded in different solvents.

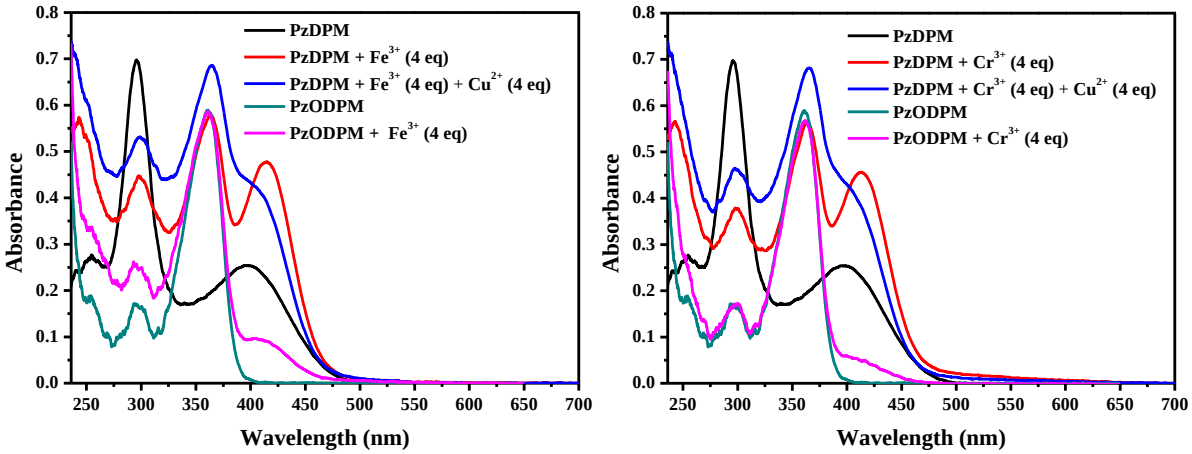

Fig. S3 UV-vis spectra of **PzDPM** (blank line) and with Fe^{3+} (left) or Cr^{3+} (right) (red line), and in the presence of both Cu^{2+} and Fe^{3+} (left) or Cr^{3+} (right) (blue line), as well as UV-vis spectra of **PzODPM** (green line) and with Fe^{3+} (left) or Cr^{3+} (right) (Magente line).

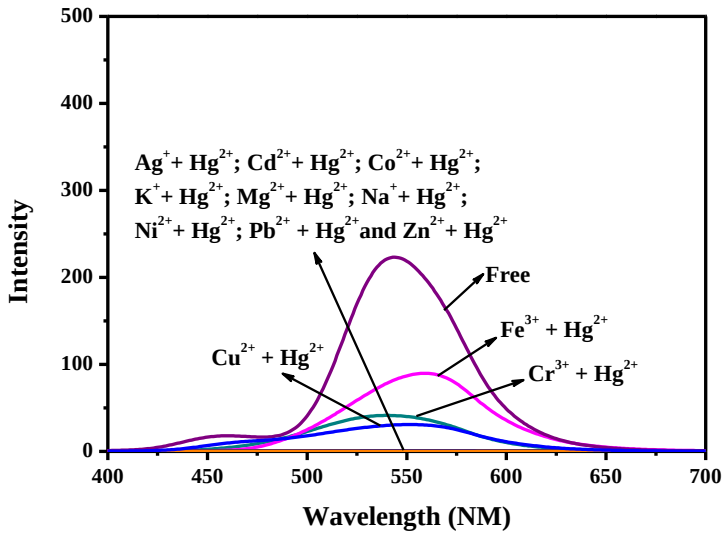

Fig. S4 Fluorescence response (λ_{ex} = 360nm) of **PzDPM** (20 μM) to 4 equiv of Hg^{2+} in MeCN containing stated metal ions. Metal ions: Ag^{+}, Cd^{2+}, Co^{2+}, Cr^{3+}, Cu^{2+}, Fe^{3+}, K^{+}, Mg^{2+}, Na^{+}, Ni^{2+}, Pb^{2+}, Zn^{2+}.

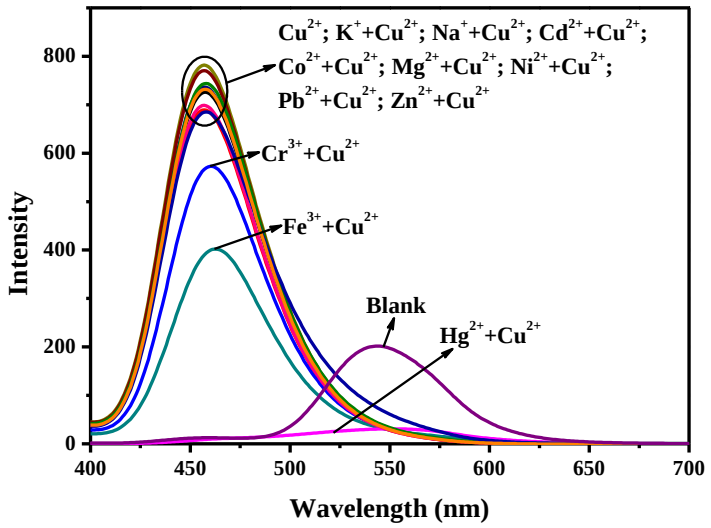

Fig. S5 Fluorescence response (λ_{ex} = 360nm) of **PzDPM** (20 μM) to 4 equiv of Cu^{2+} in MeCN containing stated metal ions. Metal ions: Ag^{+}, Cd^{2+}, Co^{2+}, Cr^{3+}, Hg^{2+}, Fe^{3+}, K^{+}, Mg^{2+}, Na^{+}, Ni^{2+}, Pb^{2+}, Zn^{2+}.

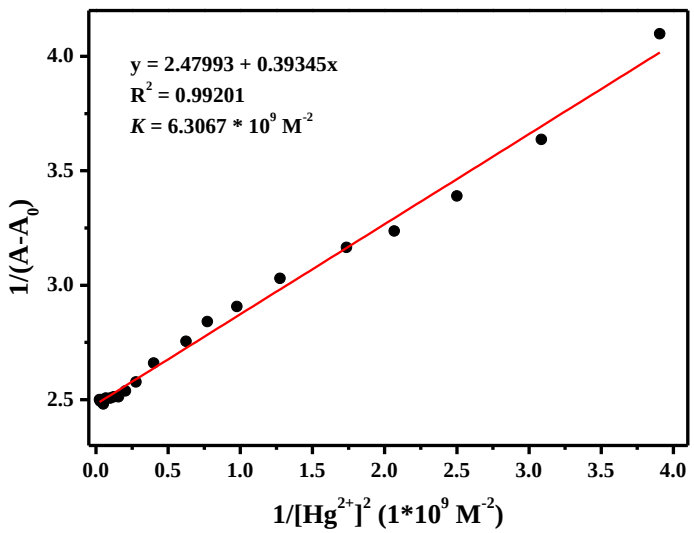

Fig. S6 Benesi−Hildebrand plot (absorbance of 500 nm) of **PzDPM** toward Hg^{2+}, assuming 1:2 stoichiometry of association between **PzDPM** and Hg^{2+}. The Benesi−Hildebrand equation is given as follows: $\frac{1}{A-A_0} = \frac{1}{K(A-A_0)[Hg^{2+}]^2} + \frac{1}{A_{max}-A_0}$

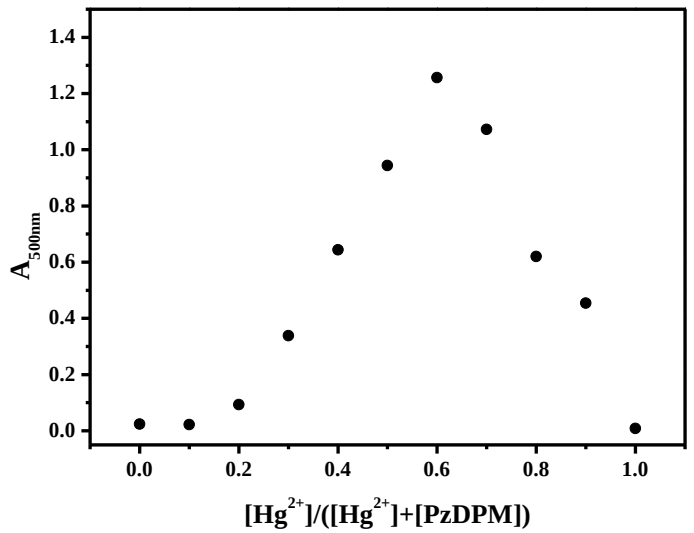

Fig. S7 Job's plot for evaluation of the 2:3 binding stoichiometry between **PzDPM** and Hg^{2+} in MeCN. The total concentration of **PzDPM** and Hg^{2+} is 200 μM.

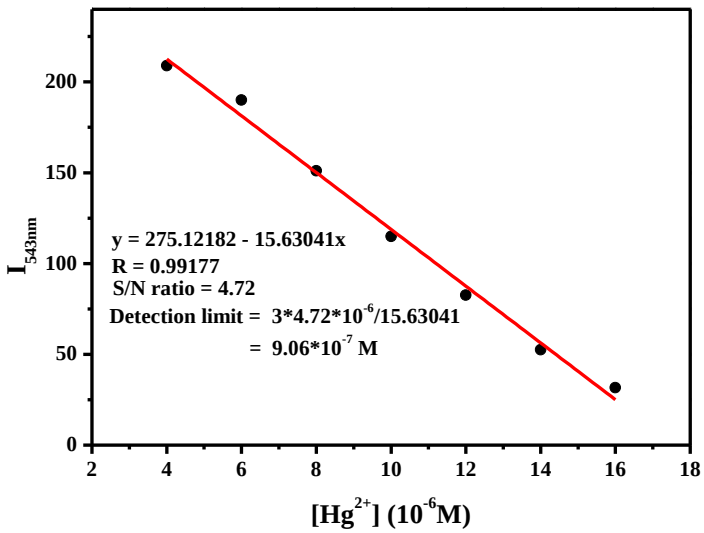

Fig. S8 Calculation process of the detection limit of **PzDPM** toward Hg^{2+}.

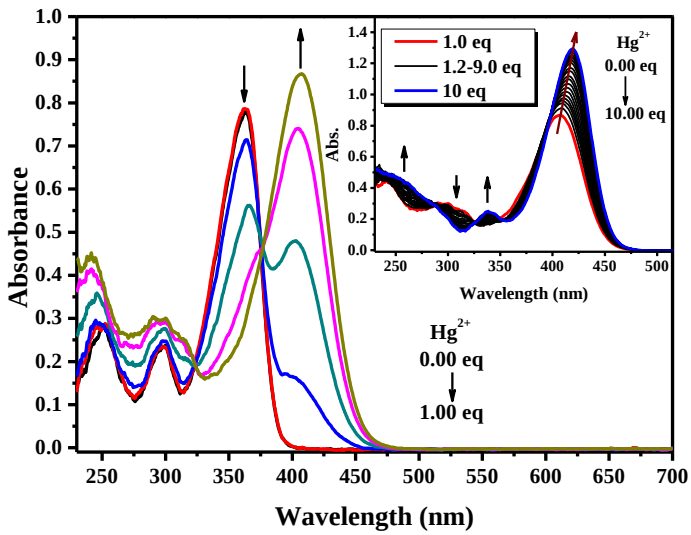

Fig. S9 Changes in absorption spectra of **PzODPM** (20 μM) in MeCN with various amounts of Hg^{2+} ions (λ_{ex} = 360 nm) after 3 min. Inset of: absorption spectra of **PzODPM** (20 μM) in MeCN in the presence of 1.0 − 10.0 equiv of Hg^{2+} ions after 3 min.

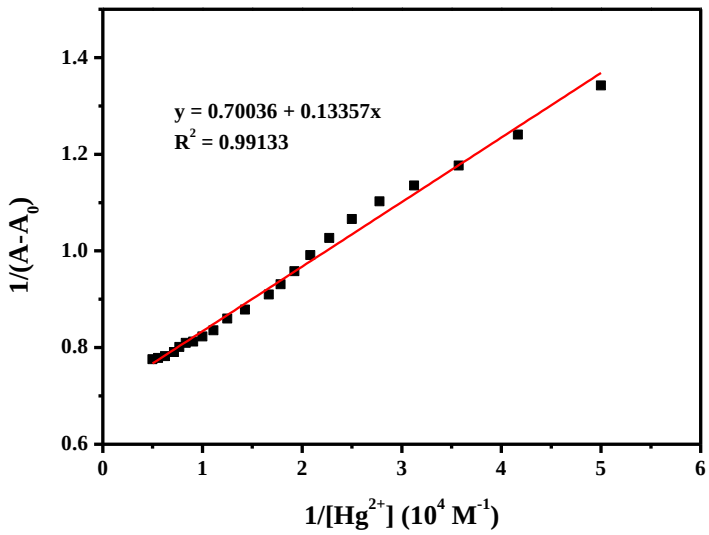

Fig. S10 Benesi−Hildebrand plot (absorbance of 419 nm) of **PzODPM** toward Hg^{2+}, assuming 1:1 stoichiometry of association between **PzODPM** and Hg^{2+}. The Benesi−Hildebrand equation is given as follows: $\frac{1}{A-A_0} = \frac{1}{K(A-A_0)[Hg^{2+}]} + \frac{1}{A_{max}-A_0}$

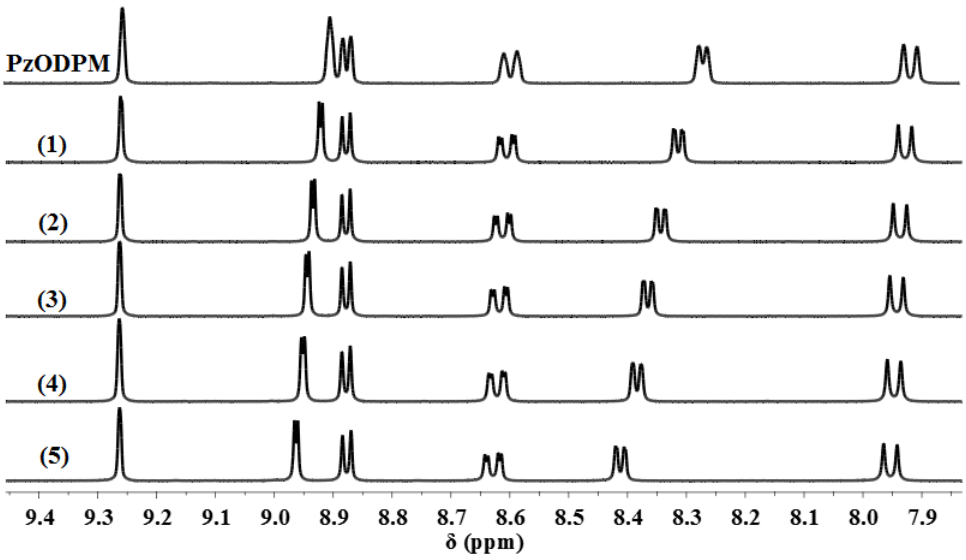

Fig. S11 Partial ^{1}H NMR (400 MHz) titrations of **PzODPM** in DMSO-d_6 with $Hg(ClO_4)_2$ in CD_3CN: (1) 0.5 equiv; (2) 1.0 equiv; (3) 2.0 equiv; (4) 3.0 equiv; (5) 4.0 equiv.

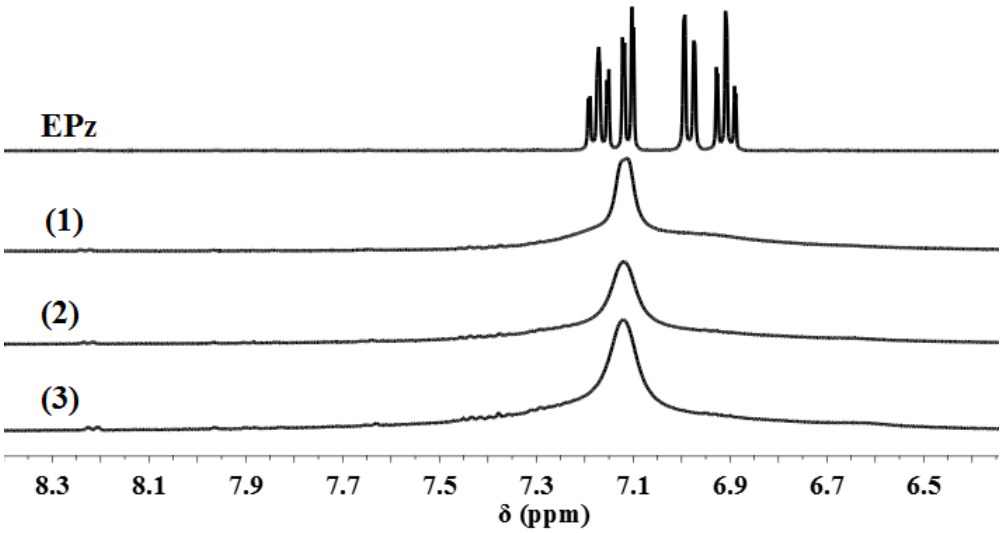

Fig. S12 Partial ^{1}H NMR (400 MHz) titrations of **EPz** in DMSO-d_6 with $Hg(ClO_4)_2$ in CD_3CN: (1) 1.0 equiv; (2) 2.0 equiv; (3) 3.0 equiv.

Fig. S13 The photograph of **PzDPM** (10 *m*M) in MeCN in the presence of Hg^{2+} (20 *m*M).

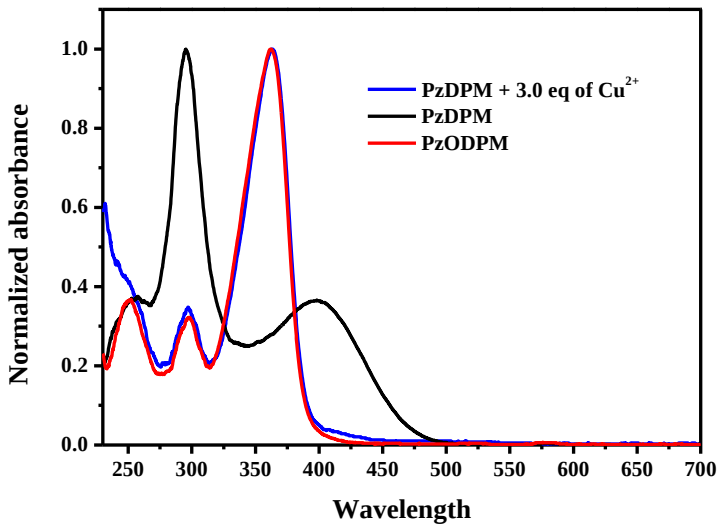

Fig. S14 Normalized UV-vis spectra of **PzDPM** without (blank line) and with Cu^{2+} (3 equiv, blue line) and **PzODPM** (red line) in MeCN.

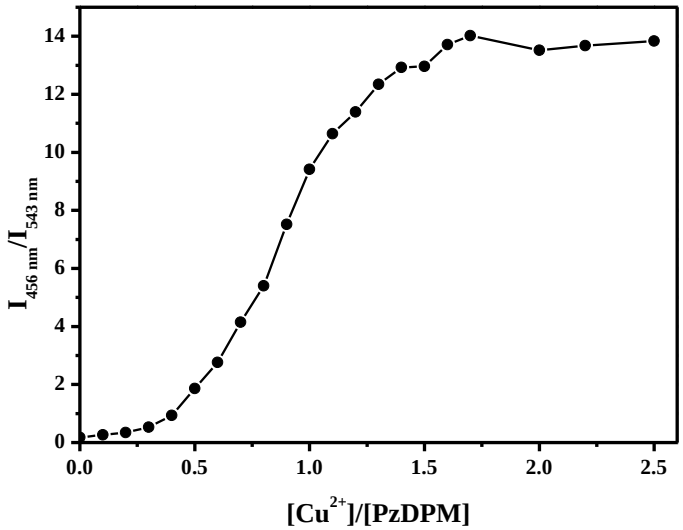

Fig. S15 The emission intensity ratio of the marked wavelength as a function of the ratio of $[Cu^{2+}]$/[**PzDPM**].

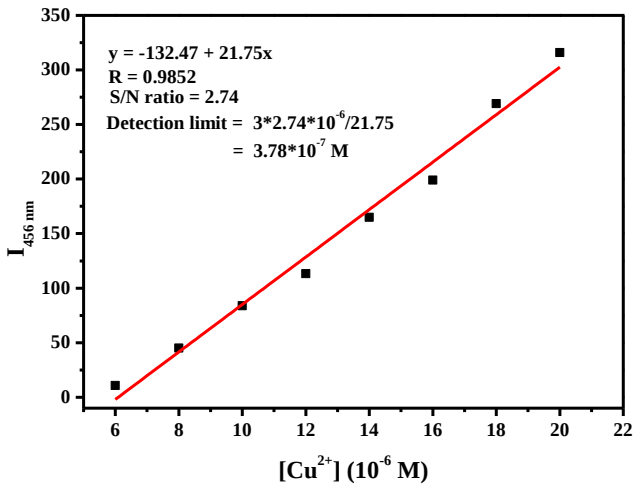

Fig. S16 Calculation process of the detection limit of **PzDPM** toward Cu^{2+}.

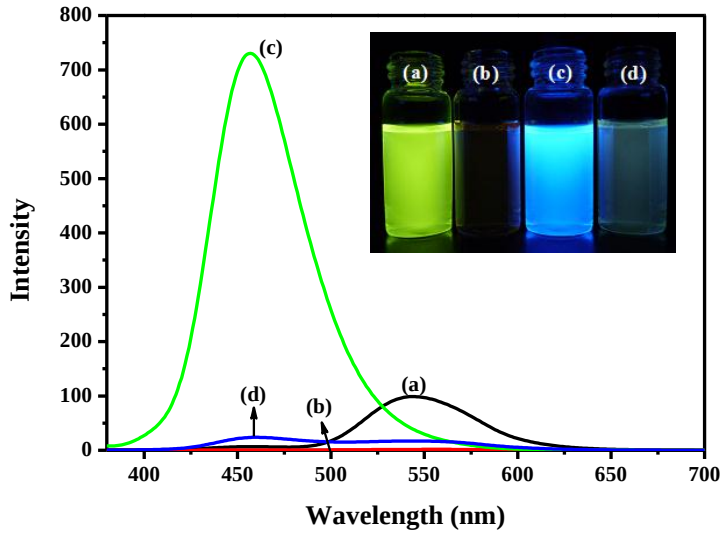

Fig. S17 Luminescence spectra (λ_{ex} = 360 nm) and emission photos (inset, λ_{ex} = 365 nm) of **PzDPM** (20 μM) in MeCN upon addition of Hg^{2+} and Cu^{2+}. (a) only **PzDPM**; (b) **PzDPM** with 2.0 equiv of Hg^{2+}; (c) **PzDPM** with 2.0 equiv of Cu^{2+}; (d) **PzDPM** with 2.0 equiv of Hg^{2+} and 2.0 equiv of Cu^{2+}.

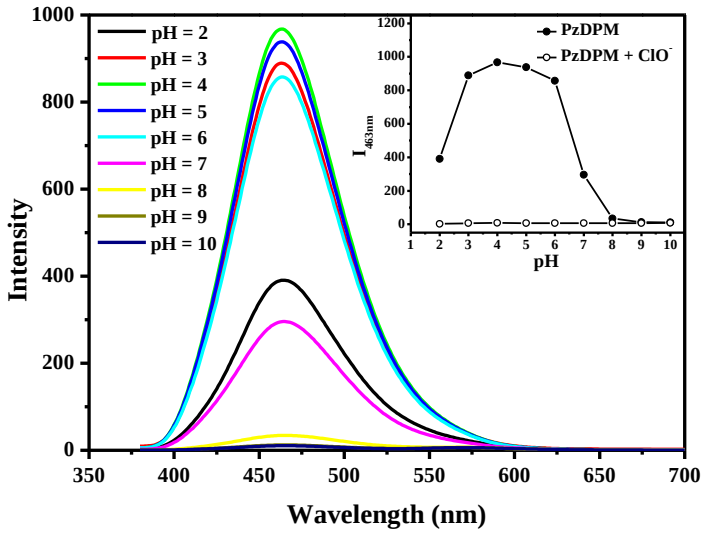

Fig. S18 Luminescence spectra (λ_{ex} = 360 nm) of **PzDPM** (10 μM) in the presence of ClO^- (0.2 *m*M) in 1 : 4 (v/v) MeCN : Tris−HCl (10 mM) with different pH value. Inset: Fluorescence intensity of **PzDPM** (10 μM) in 1 : 4 (v/v) MeCN : Tris−HCl (10 mM) with and without ClO^- (0.2 *m*M) measured as a function of pH.

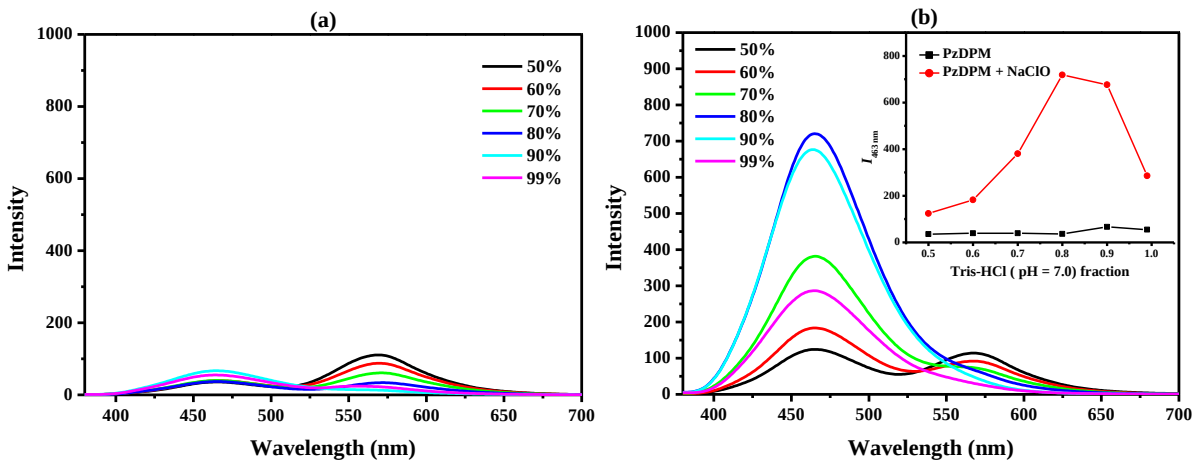

Fig. S19 Luminescence spectra (λ_{ex} = 360 nm) of **PzDPM** (10 μM) without (a) and with (b) ClO^- (0.2 *m*M) in MeCN and Tris−HCl (10 mM, pH = 7.0) mixtures with different Tris−HCl (10 mM, pH = 7.0) fractions. Inset: the profile of fluorescence intensity of **PzDPM** (10 μM) without (blank line) and with (red line) ClO^- (0.2 *m*M) *vs.* solvent composition of the MeCN and Tris−HCl (10 mM, pH = 7.0) mixtures.

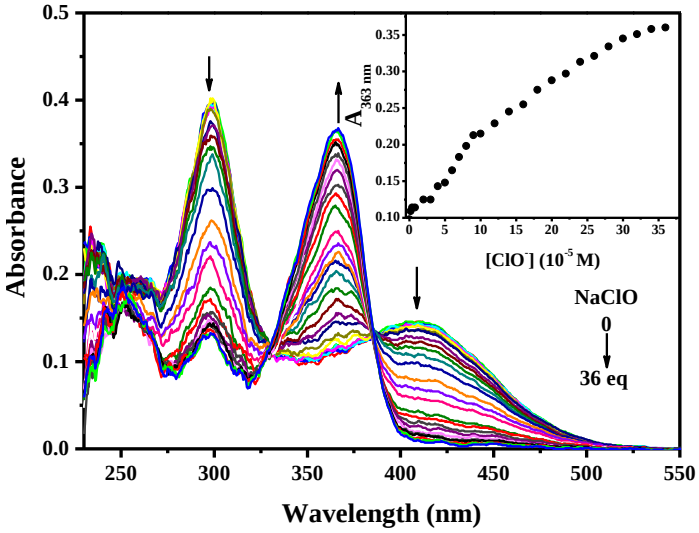

Fig. S20 Changes in absorption spectra of **PzDPM** (10 μM) in 1 : 4 (v/v) MeCN : Tris−HCl (10 mM, pH = 7.0) with various amounts of ClO^- ions (λ_{ex} = 360 nm) after 20 min. Inset of: titration curve of $A_{363\ nm}$ *vs*. ClO^- concentration.

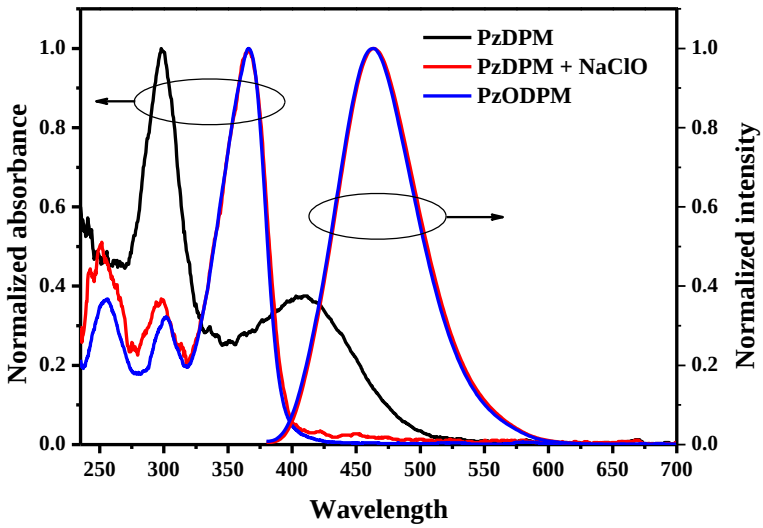

Fig. S21 Normalized UV-vis and emission spectra of **PzDPM** without (blank line) and with ClO^- (30 equiv, red line) and **PzODPM** (blue line) in 1 : 4 (v/v) MeCN : Tris−HCl (10 mM, pH = 7.0).

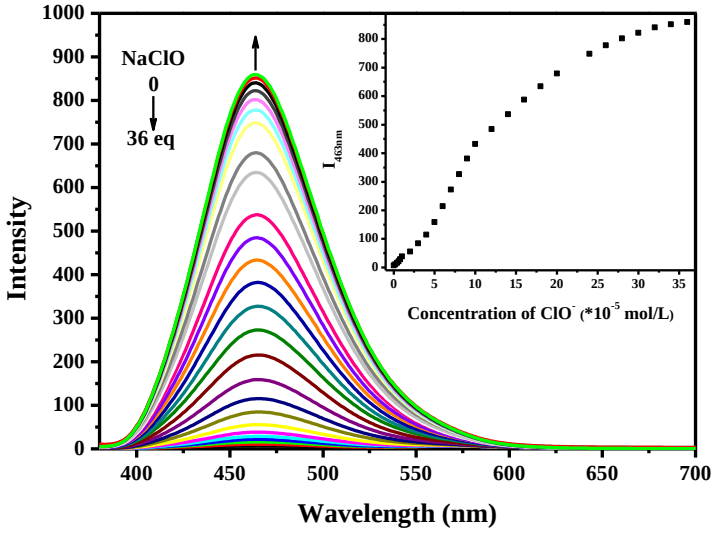

Fig. S22 Changes in emission spectra of **PzDPM** (10 μM) in 1 : 4 (v/v) MeCN : Tris−HCl (10 mM, pH = 7.0) with various amounts of ClO^- ions (λ_{ex} = 360 nm) after 20 min. Inset of: titration curve of $A_{363\ nm}$ *vs*. ClO^- concentration

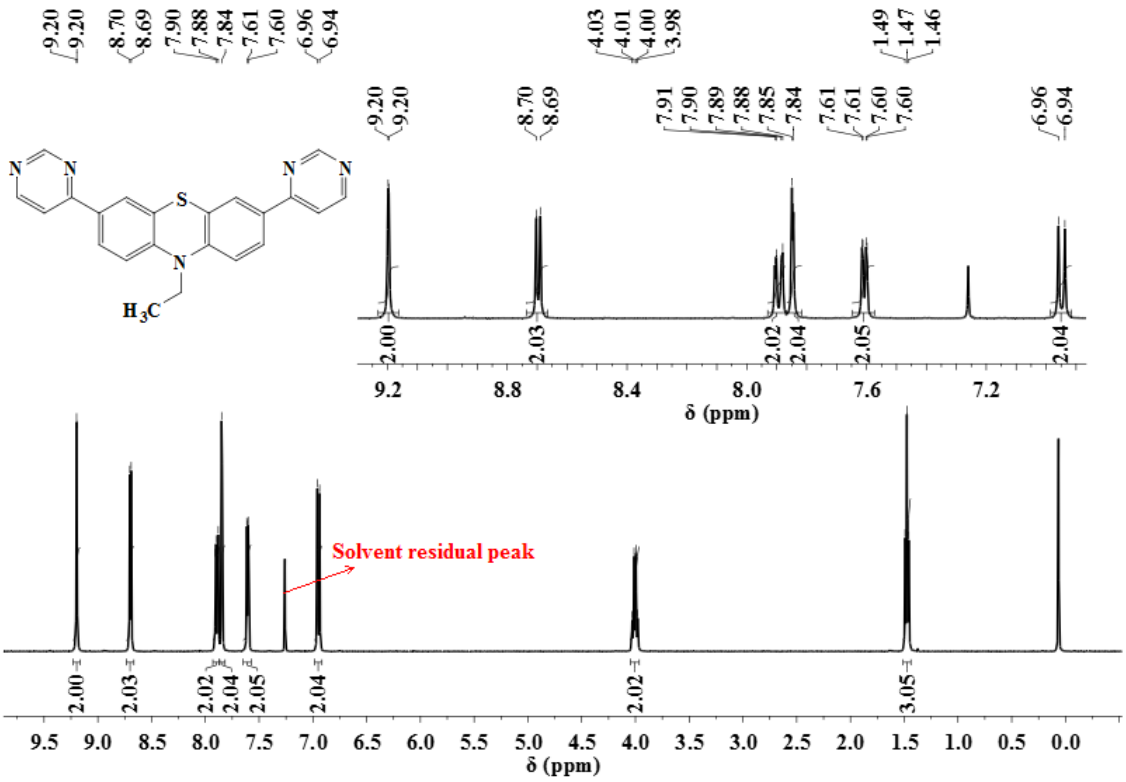

Fig. S23 ^{1}H NMR of **PzDPM** in $CDCl_3$.

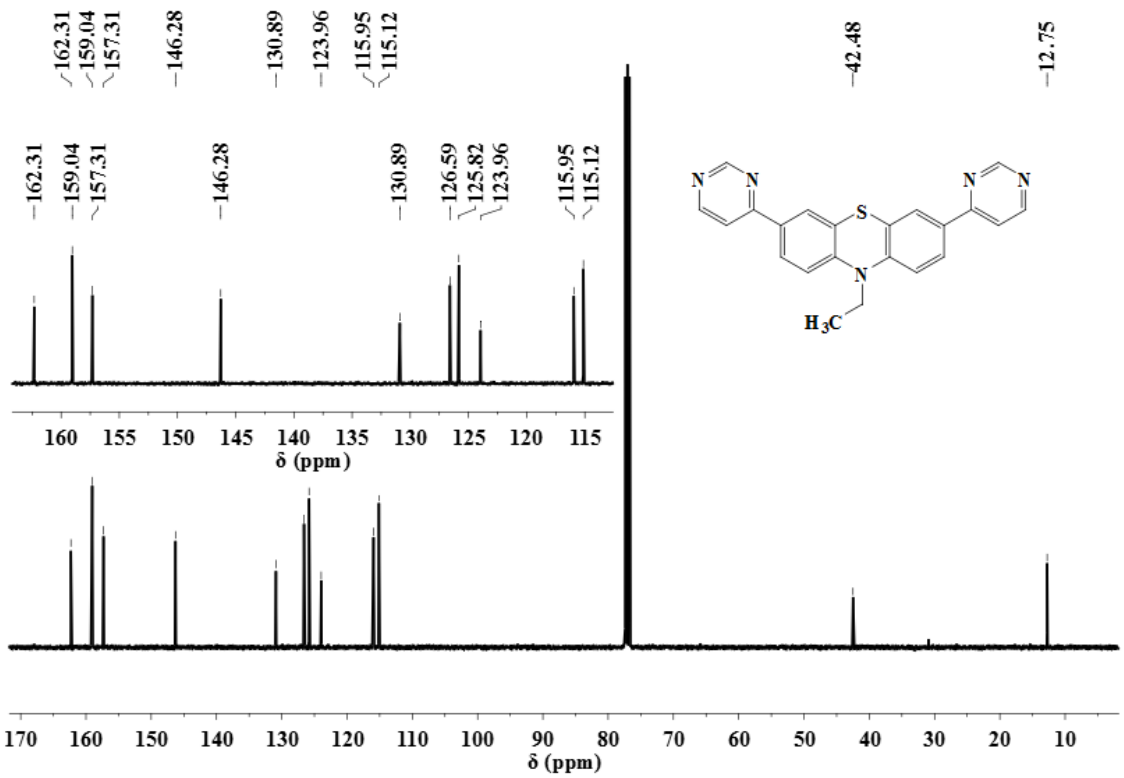

Fig. S24 ^{13}C NMR of **PzDPM** in $CDCl_3$.

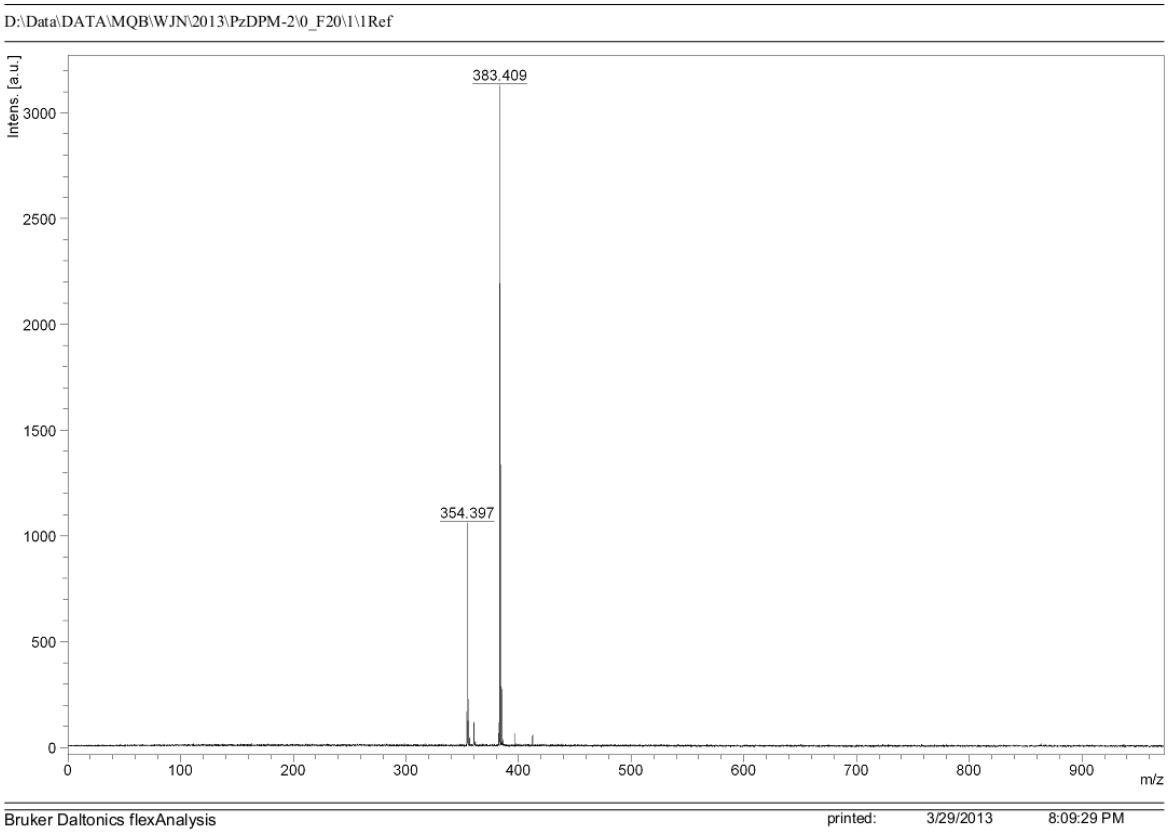

Fig. S25 MADIL-TOF mass spectrum of **PzDPM**.

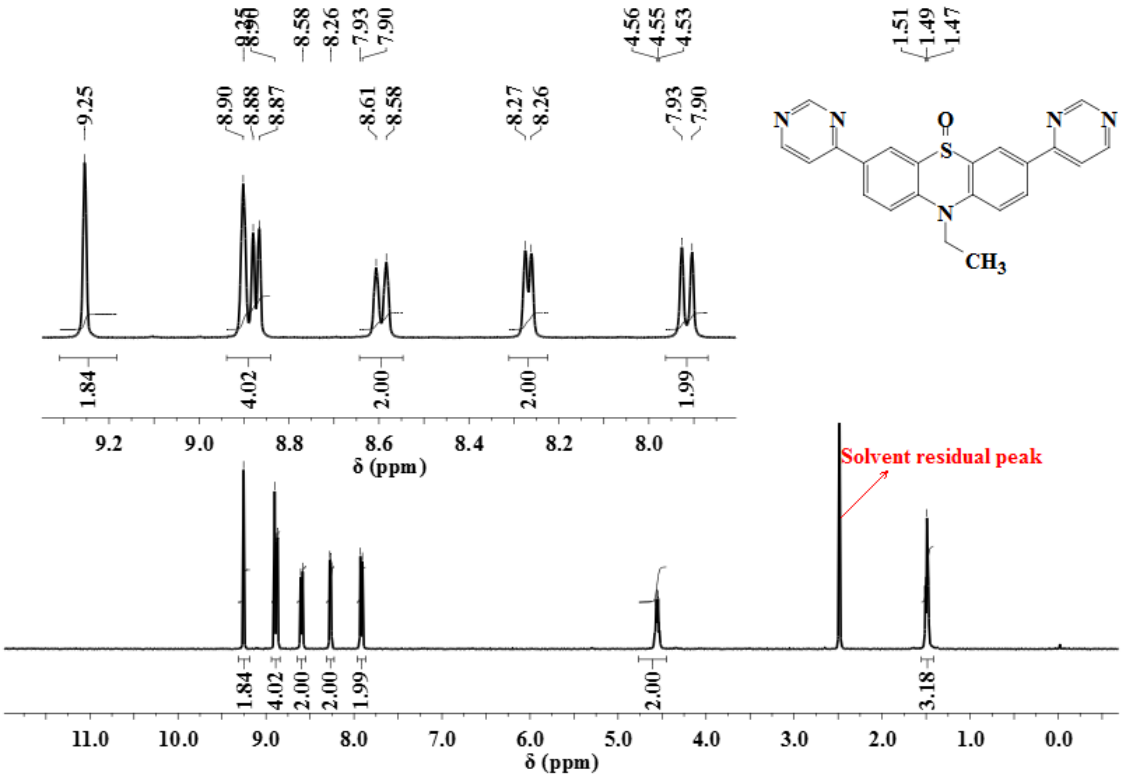

Fig. S26 ^{1}H NMR of **PzODPM** in DMSO-d_6.

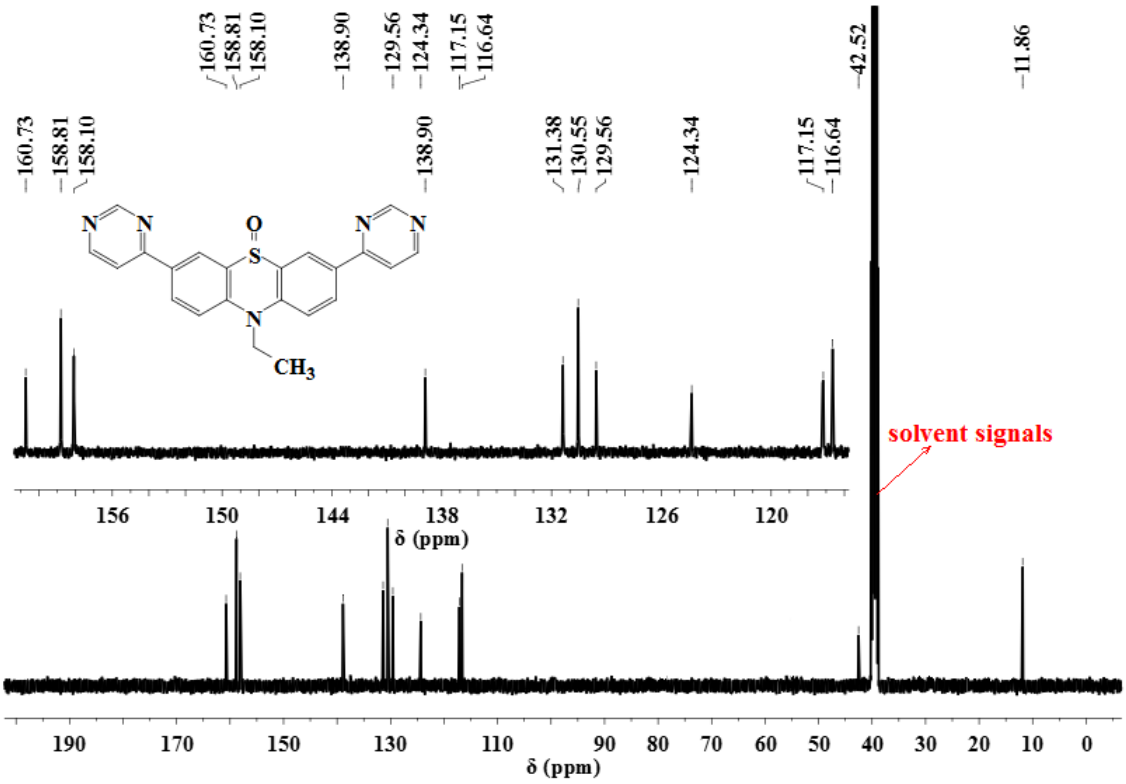

Fig. S27 ^{13}C NMR of **PzODPM** in DMSO-d_6.

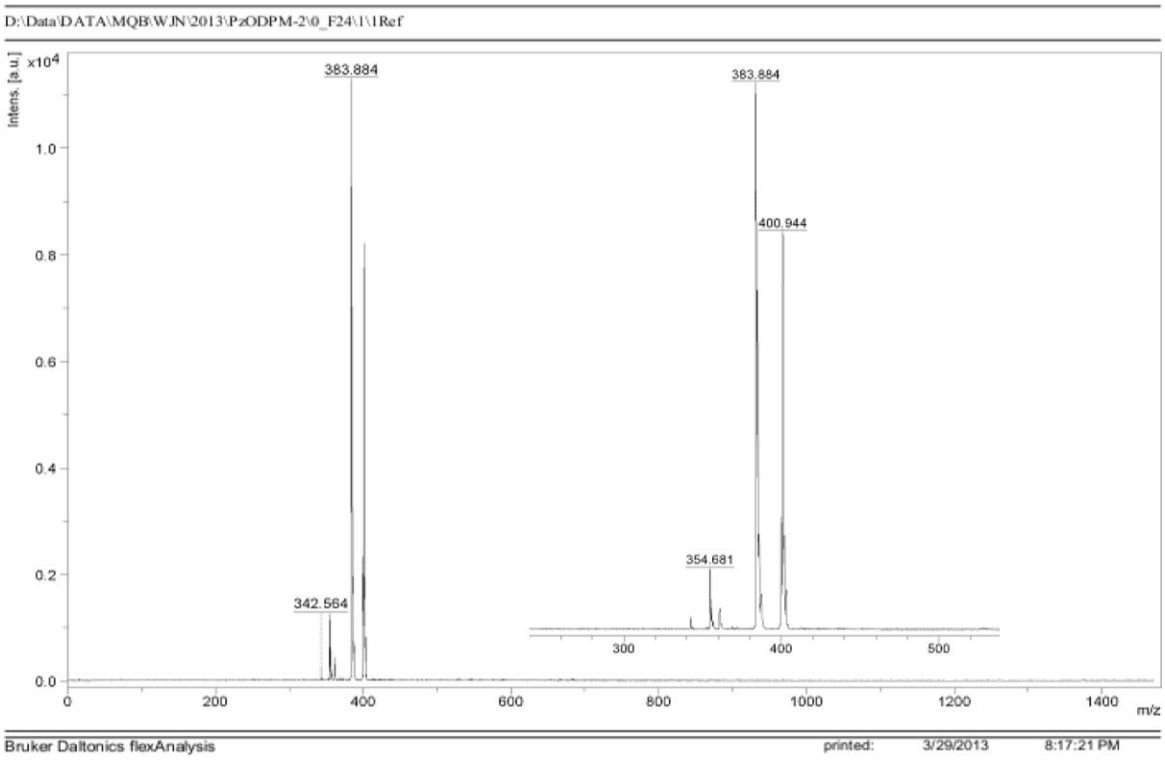

Fig. S28 MADIL-TOF mass spectrum of **PzODPM** (matrix: *trans*-2-[3-(4-tert-butylphenyl)-2-methyl-2-propenylidene] malononitrile (DCTB))